

Unusual plasma formations produced by positive streamers entering the cloud of negatively charged water droplets

Alexander Yu. Kostinskiy¹, Nikolay A. Bogatov², Vladimir S. Syssoev³, Eugene A. Mareev⁴, M. G. Andreev¹, Marat U. Bulatov³, Dmitry I. Sukharevsky³, and Vladimir A. Rakov⁵

¹National Research University Higher School of Economics

²Institute of Applied Physics of the Russian Academy of Sciences

³High-Voltage Research Center of the All-Russia Institute of Electrical Engineering

⁴Russian Academy of Sciences (RAS)

⁵University of Florida

November 26, 2022

Abstract

Kostinskiy et al. (2015a), using a high-speed infrared (2.5-5.5 μm) camera, discovered the so-called unusual plasma formations (UPFs) in artificial clouds of charged water droplets. UPFs had complex morphology including both streamer-like regions and hot channel segments. They were observed both in the presence and in the absence of hot leader channels developing from the grounded plane toward the cloud. In this paper, which is aimed at revealing the genesis of UPFs, we present two UPFs that occurred inside the initial corona streamer burst of positive polarity emitted from the grounded plane, prior to the formation (or in the absence) of associated hot leader channel. These streamer bursts developed at speeds of 5 to 7 $\times 10^5$ m/s over 1 to 1.5 m in apparently clear air before entering the negatively-charged cloud and producing UPFs at its periphery. Hot channel segments within UPFs were formed in very short times of the order of 1 μs or less. It is not clear if the UPFs were caused solely by the enhanced electric field near the charged cloud boundary or other factors also played a role. Occurrence of UPFs may be a necessary component of any lightning initiation mechanism (Kostinskiy et al., 2020; Iudin et al., 2021).

Unusual plasma formations produced by positive streamers entering the cloud of negatively charged water droplets

A. Yu. Kostinskiy¹, N. A. Bogatov², V. S. Syssoev³, E. A. Mareev², M. G. Andreev¹, M. U. Bulatov³, D. I. Sukharevsky³ and V. A. Rakov⁴

¹National Research University Higher School of Economics, Moscow, Russia,

²Institute of Applied Physics RAS, Nizhny Novgorod, Russia,

³High-Voltage Research Center of the All-Russian Scientific Research Institute of Technical Physics, Istra, Russia,

⁴Department of Electrical and Computer Engineering, University of Florida, Gainesville, FL, USA

Abstract. Kostinskiy et al. (2015a), using a high-speed infrared (2.5-5.5 μm) camera, discovered the so-called unusual plasma formations (UPFs) in artificial clouds of charged water droplets. UPFs had complex morphology including both streamer-like regions and hot channel segments. They were observed both in the presence and in the absence of hot leader channels developing from the grounded plane toward the cloud. In this paper, which is aimed at revealing the genesis of UPFs, we present two UPFs that occurred inside the initial corona streamer burst of positive polarity emitted from the grounded plane, prior to the formation (or in the absence) of associated hot leader channel. These streamer bursts developed at speeds of 5 to 7 $\times 10^5$ m/s over 1 to 1.5 m in apparently clear air before entering the negatively-charged cloud and producing UPFs at its periphery. Hot channel segments within UPFs were formed in very short times of the order of 1 μs or less. It is not clear if the UPFs were caused solely by the enhanced electric field near the charged cloud boundary or other factors also played a role. Occurrence of UPFs may be a necessary component of any lightning initiation mechanism (Kostinskiy et al., 2020; Iudin et al., 2021).

Key Points:

1. Unusual plasma formations (UPFs) can occur inside the initial corona streamer burst, before the development (or in the absence) of hot leader channel
2. UPFs contain hot channel segments that are formed, possibly via thermal-ionizational instability, on a time scale of the order of 1 μs or less
3. UPFs tend to occur in the vicinity of cloud boundary, where the electric field is highest, as this boundary is penetrated by the streamer burst

Introduction

Kostinskiy et al. (2015a,b), using a framing camera operating in the infrared (IR) range of 2.5-5.5 μm , have discovered a new class of electric discharges within artificial clouds of charged water droplets and termed them unusual plasma formations (UPFs). In the IR images, some UPF segments had similar or even greater brightness than the positive upward leader channel imaged in the same frame, suggesting that the temperature of those UPF segments is comparable to that of upward positive leaders. The upward positive leaders were preceded by initial positive corona streamer bursts, both originating from the grounded plane and propagating over 1 m or so toward the negatively charged cloud. The relatively long exposure time, 2-3 ms, of the infrared camera used by Kostinskiy et al. (2015a) did not allow them to

39 resolve the dynamics of UPFs and draw any conclusions about the mechanism of their initiation and
40 development.

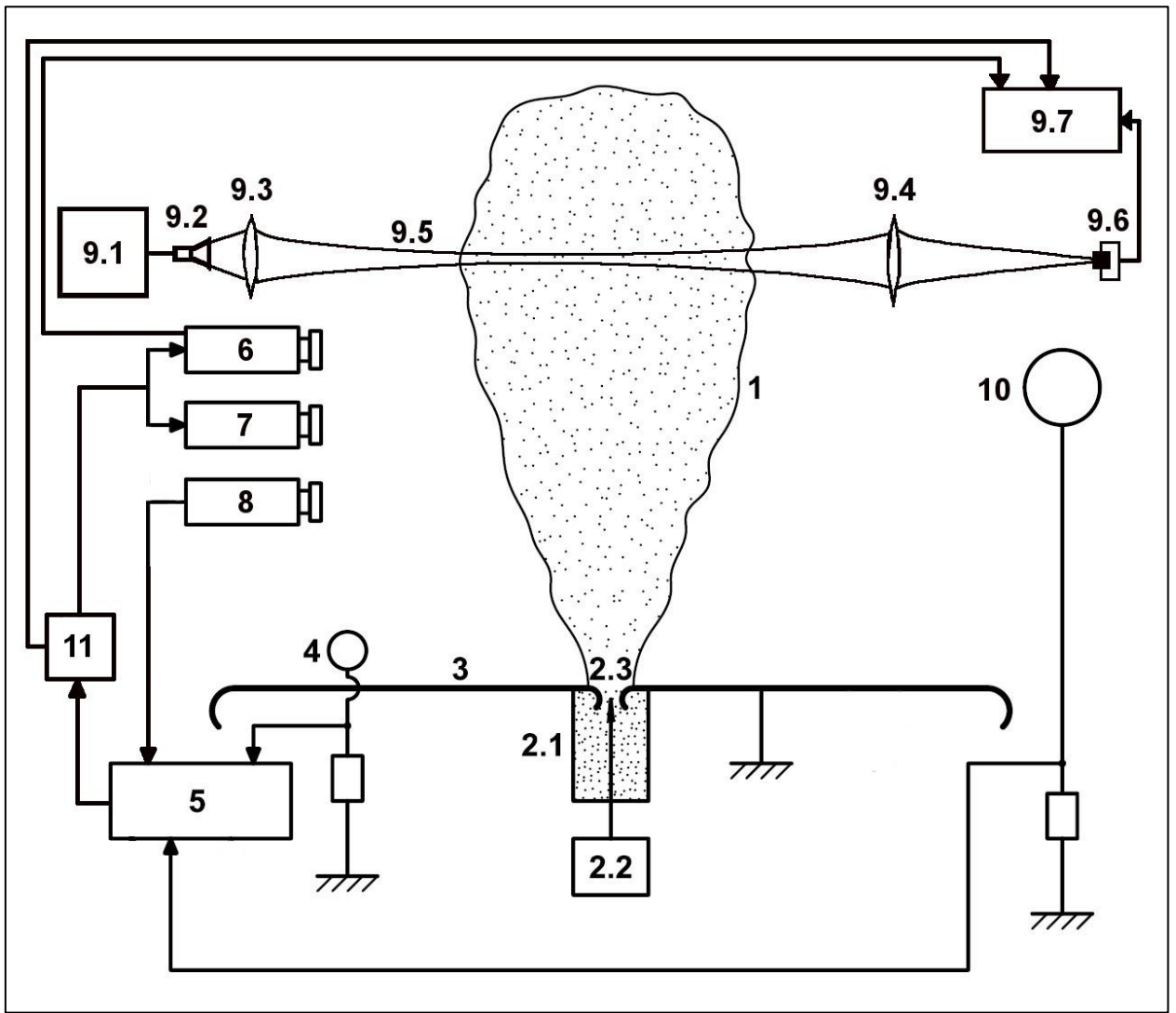
41 The goal of this work was to examine the genesis of UPFs; that is, processes that trigger their occurrence.
42 In order to accomplish this, an experimental setup used by Kostinskiy et al. (2015a), was supplemented
43 by microwave diagnostics (Bogatov et al., 2020), which, together with other devices, provided
44 experimental data that allowed us to reveal a possible mechanism of the occurrence of UPFs.

45 In this article, we use the term “long streamers” in referring to streamers that have essentially lost their
46 galvanic (electrical) connection with their origin. Streamer is a cold plasma formation composed of a
47 brighter head and a much fainter tail. Part of the tail, which is closer to the head, contains a significant
48 number of free electrons and therefore is conducting. The characteristic length of the conducting part of
49 streamer tail can be estimated based on the speed of movement of streamer head v_{str} and the electron
50 attachment time τ_a in the streamer channel behind the head: $L_{str} \approx v_{str}\tau_a = 2 - 10 \cdot 10^7 \frac{cm}{s} \cdot 10^{-7} s \approx$
51 $2 - 10 \text{ cm}$ (Bazelyan & Raizer, 1998; Kossyi et al., 1992). Thus, streamers whose heads moved farther
52 than 1 – 10 cm from their origin are considered here as long streamers.

53 **Experimental setup**

54 The experiments were performed at the High-Voltage Research Center of the Zababakhin All-Russian
55 Scientific Research Institute of Technical Physics, Istra, (<http://www.ckp-rf.ru/usu/73578/>). The
56 experimental setup used in this study (Fig. 1) was similar to the one used in previous studies and described
57 in detail by Kostinskiy et al. (2015a,b; 2016). Charged cloud (1) was created by steam generator (2.1) and
58 high-voltage source (2.2) coupled with the corona-producing sharp point (needle). The latter was located
59 in the nozzle (2.3) which the steam-air jet was passing through. The steam in the nozzle had a temperature
60 of about 100-120 °C and a pressure in the range of 0.2–0.6 MPa. The steam moved at an initial speed of
61 about 400-420 m/s with an aperture angle of 28°, forming a submerged turbulent jet. The nozzle with the
62 needle was located in the center of a grounded plane (3) with a diameter of 2 m. As a result of rapid
63 cooling, the vapor condensed into water droplets with an average radius of about 0.5 μm. Ions produced
64 by corona discharge between the tip of the needle and the nozzle (2.3) served to charge the water
65 droplets. The corona-producing needle was energized by a 10–20 kV DC voltage source. The current
66 carried by the charged aerosol jet was in the range from 60 to 150 μA. When the total charge accumulated
67 in the cloud reached ~60 μC, meter-scale sparks spontaneously appeared between the nearby grounded
68 objects and the cloud. In the case of negatively-charged cloud, the sparks usually occurred as a sequence
69 of an initial positive corona streamer burst and a positive leader, both developing from the grounded
70 metal sphere (4) toward the cloud (1). The metal sphere had a diameter of 5 cm and was located at a
71 distance of 0.85 m from the center of the grounded plane (3). The top point of the sphere was 12 cm
72 above the plane. Initial positive corona streamer bursts and positive leaders, originating from the metal
73 sphere, propagated essentially perpendicular to the direction of the diagnostic microwave beam (9.5).

74 Currents of initial corona streamer bursts and upward positive leaders were measured by a low-
75 inductance 1-Ω shunt, inserted between the metal sphere (4) and ground, and a digitizing oscilloscope
76 (5). Once the current exceeds a preset threshold value, the oscilloscope (5) records (a) the current through
77 the shunt, (b) the discharge luminosity signal from the photomultiplier tube (PMT) (8), and (c) the signal
78 from the 50-cm diameter metal sphere (10), used for monitoring the variation of cloud charge. The
79 oscilloscope also outputs a trigger signal for the pulse generator (11) which forms a TTL pulse triggering
80 high-speed cameras 4Picos (6) and FLIR SC7700M (7), as well as a second oscilloscope (9.7) recording
81 microwave radiation (9.5) that passed through the cloud (1). The infrared framing camera FLIR SC7700M



82

83 Figure 1. Experimental setup: 1 — cloud of negatively charged water droplets, 2.1 — steam generator, 2.2
 84 — high-voltage source with corona-producing sharp point, 2.3 — nozzle, 3 — grounded metal plane, 4 —
 85 5-cm sphere connected to ground via current-measuring shunt, 5 — oscilloscope, 6 — visible-range high-
 86 speed framing camera 4Picos, 7 — infrared high-speed framing camera FLIR-7700, 8 — photomultiplier,
 87 9.1 — microwave generator G4-91, 9.2 — horn antenna, 9.3 and 9.4 — dielectric lenses, 9.5 — microwave
 88 beam, 9.6 —receiving waveguide, microwave amplifier, and a microwave diode, 9.7 — oscilloscope, 10
 89 — 50-cm sphere for monitoring variations of cloud charge, 11 — pulse generator.

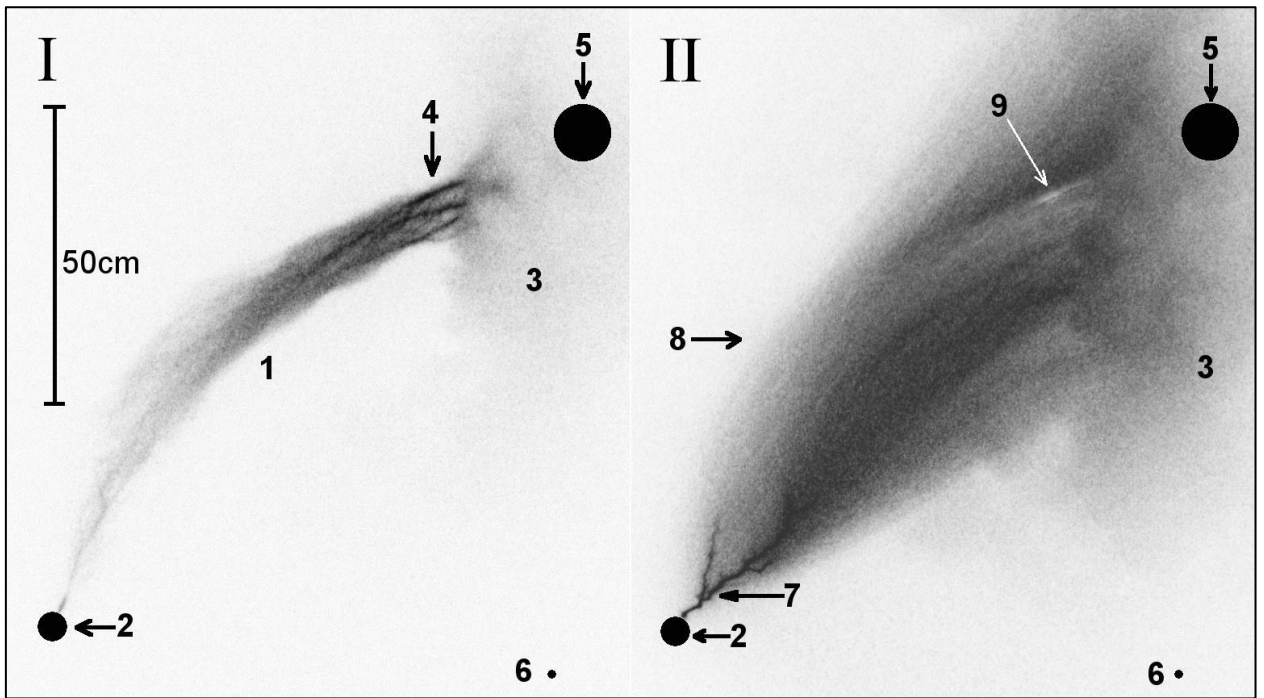
90

91 ($\lambda \approx 2.5\text{-}5.5 \mu\text{m}$) operated at 412 frames per second (exposure time was 2.4 ms), with the image size on
92 the matrix being 320×256 pixels. The IR-camera was equipped with a germanium lens with a focal length
93 of 50 mm and an aperture of f/2. The 4Picos high-speed visible-range (actually it includes a portion of the
94 UV range; $\lambda = 315\text{--}850 \text{ nm}$) camera with image amplification (optical gain was 10^4) captured images on a
95 1360×1024-pixel matrix with exposure time from 50 ns to 10 μs . It can produce only two frames with
96 selectable interframe interval of 500 ns or more. The 4Picos camera was equipped with a glass lens with
97 a focal length of 50 mm and an aperture of f/0.95. The cameras were installed at a distance of 8.5 m from
98 the nozzle, which forms the aerosol cloud (2.3) in the direction of the propagation axis of the microwave
99 beam. The viewing angle (directional diagram) of the photomultiplier was $\sim 10^\circ$, and the size of the
100 photomultiplier's field of view at the location of the cloud was $\sim 1 \text{ m}^2$. The photomultiplier tube was aimed
101 at the upper half of the cloud, at a height of about 0.8-1 m above the plane. The time constant of the PMT
102 was several milliseconds, but still it could fairly accurately record the onset of luminosity in its field of
103 view.

104 The source of microwave radiation was a G4-91 generator (9.1). The generator output power was 5 mW,
105 and the radiation frequency was 35 GHz ($\lambda = 8.5 \text{ mm}$). The generator was operating in continuous mode.
106 A converging microwave beam with a Gaussian profile was formed by a horn antenna (9.2) and dielectric
107 lenses (9.3 and 9.4). The waist of the microwave beam (9.5) was located on the axis of the cloud. The
108 angle between the axis of the microwave beam and the axis of the cloud was 85-87°. The diameter of the
109 microwave beam in the waist region was $\sim 10 \text{ cm}$ (in the studied region, the beam was almost cylindrical,
110 and in the region of the visible edge of the aerosol cloud it was only 3% wider than at its center). The
111 distance from the axis of the microwave beam to the grounded plane was $\sim 1 \text{ m}$. The polarization of
112 microwave radiation was linear (vertical). Microwave radiation transmitted through the cloud was
113 focused by a dielectric lens (9.4) into the open end of the receiving waveguide, amplified with a 20 dB
114 microwave amplifier, and detected with a microwave diode (9.6). The output level of the signal from the
115 microwave diode was recorded with an oscilloscope (9.7). The relative attenuation of microwave radiation
116 passing through the cloud was determined by the ratio of the value of the output signal level from the
117 diode to the unperturbed level (in the absence of the cloud). The main source of noise that determines
118 the sensitivity of microwave diagnostics in general was the instability of the output power of the
119 microwave generator, which was $\sim 10^{-3}$; the latter value determined the minimum relative attenuation
120 of the probing microwave radiation that we could register. An uncharged cloud and a charged cloud in
121 the intervals between in-cloud events did not noticeably attenuate the probing microwave radiation. The
122 equipment was installed in three electromagnetically shielded structures/enclosures, of which two
123 smaller ones (housing the high-speed cameras 6 and 7 and the receiving part of the microwave diagnostics
124 setup 9.6; see Fig. 1) had autonomous power supply.

125 **Experimental results**

126 Presented in Fig. 2 is a sequence of two 4Picos frames separated by a time interval of 1 μs . The first frame
127 (labeled I; exposure time of 2 μs) shows the initial corona streamer burst that originated from the
128 grounded sphere in the lower left corner and entered the negatively-charged cloud in the upper right
129 corner. Also seen in the first frame is a UPF containing three bright channel segments, which are similar
130 to those reported by Kostinskiy et al. (2015a) and inferred by them to be hot (having gas temperature
131 similar to that of leader channels; it is in this sense that we refer to those segments being "hot"). The
132 second frame (labeled II; exposure time of 10 μs) shows the upward positive leader composed of a
133 relatively short, branched hot channel and a relatively large streamer zone which enters the cloud in the
134 upper right corner. Clearly, the UPF occurred inside the initial corona streamer burst, before the



135
 136
 137
 138
 139
 140
 141
 142
 143
 144
 145

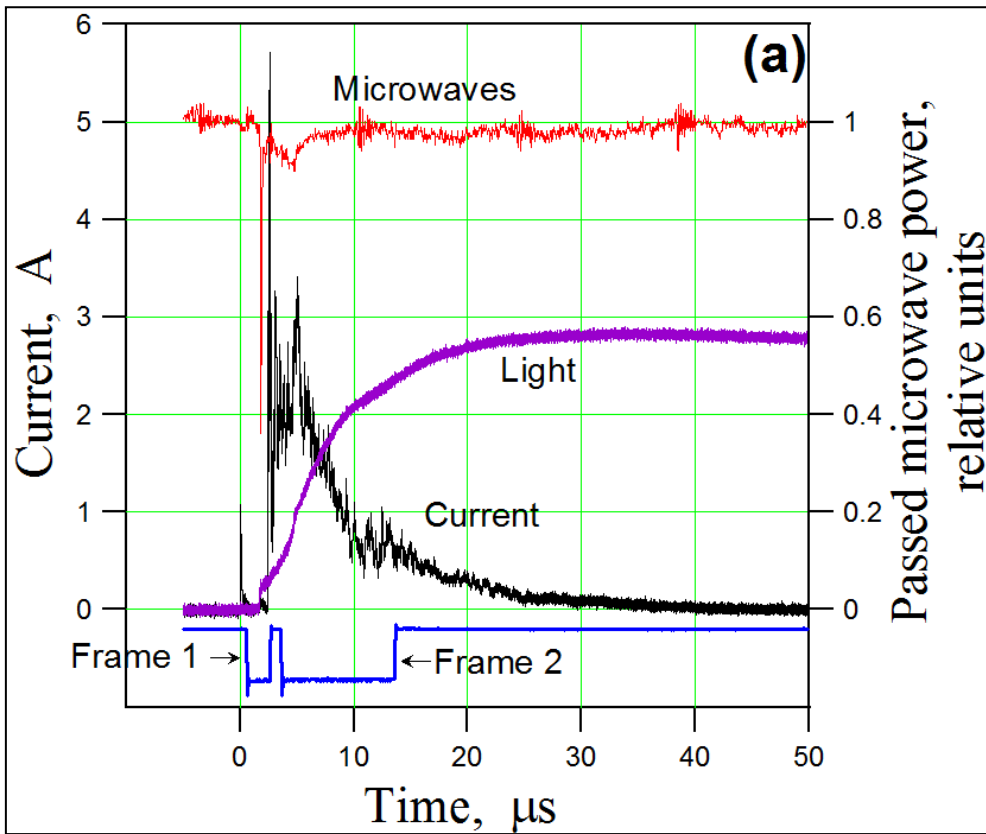
Figure 2. Two consecutive frames of event 2015-12-04_03 obtained with a visible-range 4Picos camera with image enhancement. Frames I and II had 2- μ s and 10 μ s exposure times, respectively, and the time interval between frames was 1 μ s. Both frames are inverted. 1, the initial positive corona streamer burst converted to UPF; 2, 5-cm grounded sphere equipped with a current-measuring shunt; 3, cloud of negatively charged water droplets; 4, hot channel segments embedded in UPF; 5, the region of passage of the microwave beam; 6, the center of the grounded plane where the nozzle (see Fig. 1) is located; 7, channel of upward positive leader; 8, streamer zone of the upward positive leader; and 9 - light stripe, which is an image artifact.

146 development of hot leader channel from the grounded sphere. Further, it occurred in the vicinity of the
147 visible cloud boundary, where the electric field is expected to be highest, as that boundary was penetrated
148 by the streamer burst. It is logical to assume that the streamer burst entering the cloud experienced some
149 kind of instability (for example, thermal-ionizational instability (Nighan, 1977; Raizer, 1991, pp. 222-226;
150 Bychkov et al., 2007; Zhong et al., 2019; Wolf et al., 2020)) that led to its conversion to UPF. In the
151 following, we will use the entirety of our experimental data (see Figs. 3 and 4) to estimate the time needed
152 for conversion of streamer burst to UPF seen in Fig. 2. An additional example of such conversion is
153 presented in Figs. 5a and b.

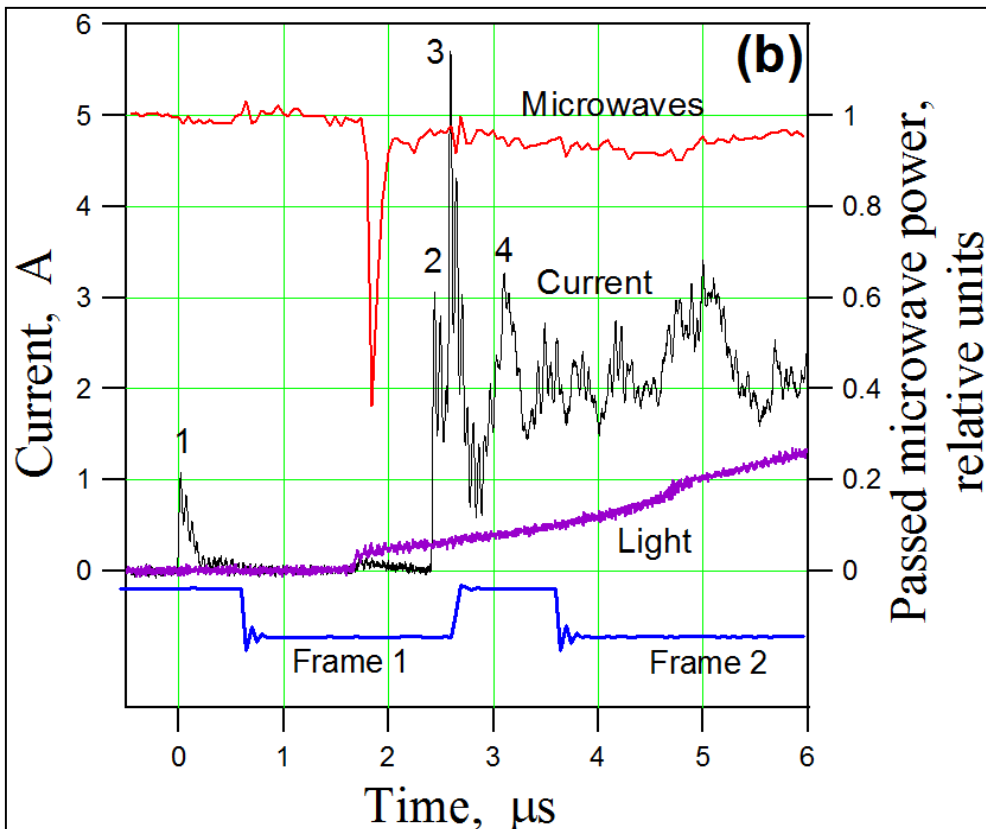
154 The initial corona streamer burst precedes the formation of hot leader channel (this is why it is referred
155 to as initial), although sometimes no following leader is formed. Current associated with those two
156 processes in the first event we are going to present exhibits the initial pulse labeled 1 Fig. 3b followed by
157 a time interval with very low current level and then by a much larger in amplitude and longer in duration
158 current waveform with multiple peaks or superimposed pulses (the overall current waveform is best seen
159 in Fig. 3a), the first three of which are labeled 2, 3, and 4 in Fig. 3b. Current pulse 1 occurred before the
160 first 4Picos frame and current peaks 2 and 3 occurred during that frame, which shows no leader channel.
161 Therefore, we attribute current pulse 1 and current peaks 2 and 3 to the initial corona streamer burst,
162 while current peak 4 and the following part of the large current waveform could be formed in the presence
163 of leader channel. It is likely that the UPF was associated with current pulse 1. Note that there is a small
164 pulse during the low-current interval, which appears to coincide with the onset of the photomultiplier
165 signal originating from the upper part of the cloud. It is not clear if it was just a minor variation of the low-
166 level current or it was somehow related to the streamer burst to UPF conversion process. Interestingly,
167 the small current pulse seems to be coincident with the beginning of appreciable cloud-charge variation
168 (not shown here), detected with 50-cm sphere 10 (see Fig. 1).

169 One can see in Fig. 2(I) those streamers of the initial corona streamer burst (1), once they entered the
170 cloud (3), were moving toward the microwave beam (5). The fact that the streamers did reach the position
171 of microwave beam is evidenced by a pronounced microwave absorption pulse with an FWHM of about
172 135 ns and its peak being within the exposure time of the first 4Picos frame (left frame labeled I in Fig. 2),
173 approximately 0.85 μs before the end of exposure of that frame. It is worth noting that corona streamers
174 in long sparks cause stronger absorption of microwave radiation than leader channels (Bogatov et al.,
175 2020). The streamer heads traversed an arc-like trajectory between the grounded sphere (2) and the
176 region of the microwave beam (5) in the cloud (3). The length of that trajectory was about $S_{st} \approx 1.2$ m and
177 the streamer-head travel time was about $\tau_{st} \approx 1.7$ μs (estimated as the time interval between the peak of
178 the current pulse 1 (see Fig. 3b), associated with the onset of the initial corona streamer burst at the
179 grounded sphere, and the onset of microwave absorption signal. Thus, the average 2D speed of streamers
180 of the initial corona streamer burst was about $v_{st} \approx S_{st}/\tau_{st} \approx 7 \cdot 10^5$ m/s.

181 Also seen in Fig. 2(I) is a UPF with three bright channel segments (4), which are partially outside of the
182 optically opaque part of the cloud and are similar to those recorded in previous experiments by Kostinskiy
183 et al. (2015a) and inferred by them to be relatively hot. Since the bright segments of UPFs are located at
184 a distance of about 1 m from the origin of the initial corona streamer burst (grounded sphere), and the
185 average velocity of streamer propagation is about 7×10^5 m/s, the process of transition of streamer burst
186 to UPF began approximately 1.4 μs ($1 \text{ m}/7 \times 10^5 \text{ m/s}$) or more after the start of the initial corona streamer
187 burst. The time interval between the onset of the initial corona streamer burst (current pulse labeled 1 in
188 Fig. 3b) and the end of exposure of the first frame of 4Picos was 2.5 μs . Since the UPF was formed before
189 the end of the exposure of this frame, its formation process took no more than 1.1 μs ($2.5 \mu\text{s} - 1.4 \mu\text{s}$).



190



191

192 Figure 3 (event 2015-12-04_03). (a) Current measured at the grounded sphere (shown in black);
 193 absorption of microwave radiation that passes through the cloud (shown in red and labeled
 194 "Microwaves"); photomultiplier signal (shown in purple and labeled "Light"), and exposure times of 4Picos
 195 Frames 1 and 2 (shown in blue and labeled I and II in Fig. 2). (b) Same as (a), but shown on an expanded
 196 time scale. The first four major current pulses are numbered in (b).

197 In the second frame of 4Picos (right frame labeled II in Fig. 2), the channel of upward positive leader (7)
 198 and its streamer zone (8) are clearly visible. The maximum 2D extent of the leader channel, measured
 199 from its origin on the grounded sphere (2) to its most distant point is about 29 ± 2 cm. It was found from
 200 the corresponding infrared images (discussed later in this paper), captured with much longer (2.4 ms)
 201 exposure time, that the total leader channel length was 42 ± 1 cm; that is, it did not enter the cloud.

202 As noted above, current pulse 1 associated with the beginning of the initial corona streamer burst was
 203 followed, after a time interval of $2.4 \mu\text{s}$, by a multi-peak current waveform. Light emissions of streamers
 204 associated with the first two peaks of that current waveform (labeled 2 and 3 in Fig. 3b) were likely imaged
 205 in the first frame of 4Picos (see Fig. 2(I)). We argue that the UPF occurred before those two subsequent
 206 streamer bursts, because the onset of signal from the photomultiplier (viewing the upper part of the
 207 cloud, with the region within about 0.5 m of the grounded sphere being outside of its field of view) was
 208 $\sim 1.7 \mu\text{s}$ after the current pulse 1 and $1.9 \mu\text{s}$ before the current pulse 2. Further, the light intensity of a
 209 discharge near the grounded sphere after being scattered by the cloud was below the sensitivity threshold
 210 of the photomultiplier. Thus, current measured at the grounded sphere must precede (not follow) the
 211 light emission detected by the photomultiplier, which means that the UPF seen in Fig. 2(I) was caused by
 212 the streamer burst associated with current pulse 1 (see Fig. 3b), as stated above.

213 Characteristics of current pulses 1 through 4 (see Fig. 3b) are summarized in Table 1.

214 Table 1. Characteristics of current pulses 1 through 4 labeled in Fig. 3b.

| | Peak current, A | Rise Time, ns | FWHM, ns | Fall Time, ns | Interpulse interval relative to pulse 1, μs |
|---------|------------------------|----------------------|-----------------|----------------------|--|
| Pulse 1 | 1.1 | 30 ± 5 ns | 90 ± 10 | 147 ± 10 | — |
| Pulse 2 | 3.14 | 30 ± 5 ns | — | — | 2.42 |
| Pulse 3 | 5.8 | 30 ± 5 ns | 130 ± 10 | 180 ± 20 | 2.58 |
| Pulse 4 | 3.3 | 195 ± 10 | 180 ± 10 | 210 ± 10 | 3.08 |

215

216 Rise time of current pulse 4 is considerably larger than that of the preceding three pulses, which might be
 217 indicative of the streamer-to-leader transition (Bazelyan and Raizer, 1998) around the time of pulse 4.
 218 With an uncertainty less than $0.2 \mu\text{s}$, the microwave absorption peak occurred $1.75 \mu\text{s}$ after current pulse
 219 1 (associated with the streamer burst, within which the UPF was formed (see Fig. 2(I)), $0.56 \mu\text{s}$ before the
 220 beginning of pulse 2, and $0.71 \mu\text{s}$ before pulse 3, after which the upward positive leader was initiated from
 221 the grounded sphere (see Fig. 2(II)).

222 The total positive charge transferred to the cloud by the initial corona streamer burst in its entirety and
 223 by the following upward leader, estimated by integrating the current waveform from 0 to $50 \mu\text{s}$, was 15
 224 μC , which is about a quarter of the typical total (negative) cloud charge.

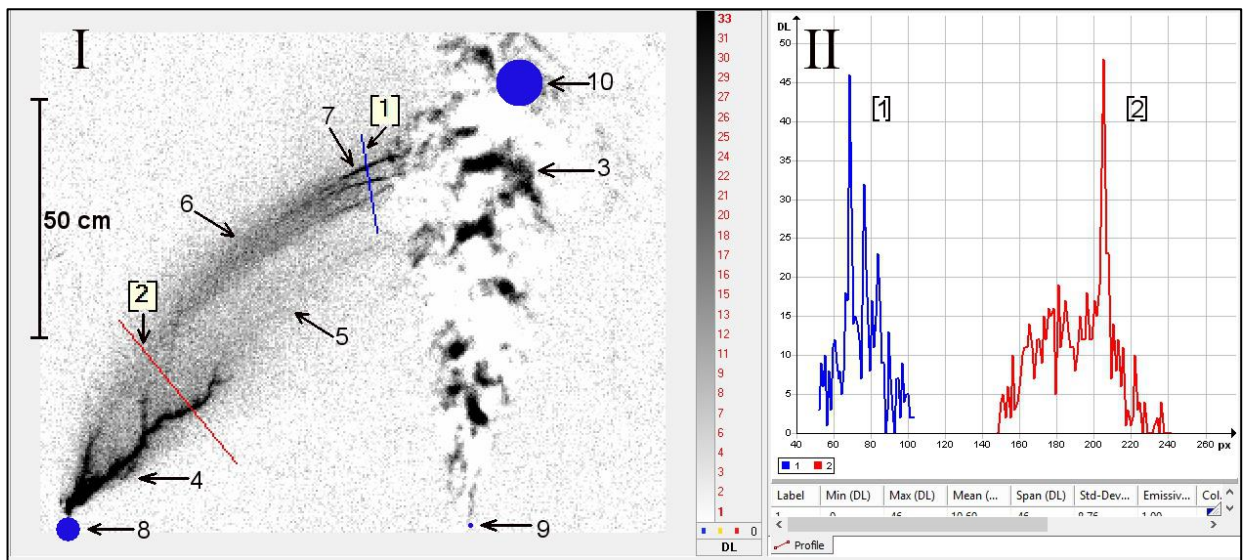
225 The upward positive leader is clearly imaged during the $10\text{-}\mu\text{s}$ exposure time of the second 4Picos frame
 226 (see Fig. 2(II)). For the first couple of microseconds, when the leader current was 2-3 A, some of the
 227 streamers apparently reached the region of passage of the microwave beam (labeled 5 in Fig. 2(II)), as
 228 evidenced by the small absorption of microwave radiation seen in Fig. 3. Interestingly, the absorption is
 229 smaller for current pulse 3, whose peak is appreciably larger (5.8 A). The latter observation may indicate
 230 that most of the streamers did not reach the microwave beam.

231 Fig. 4(I) shows an infrared (IR) image of the event whose visible-range image is shown in Fig. 2. In Fig. 4(I),
232 the image size is 320 x 256 pixels, and frame exposure time is 2.4 ms). To improve contrast, the presented
233 IR image was obtained by subtracting the previous frame from this one and inverted. With the exposure
234 time of 2.4 ms, almost all discharge processes are imaged (integrated) in the presented single (differential)
235 frame. The relatively hot channel (4) of the branching upward positive leader and its streamer zone (5)
236 reaching the cloud are superimposed on the image of the preceding initial corona streamer burst/UPF (6)
237 with relatively hot channel segments (7). Overall, the IR image is similar to its visible-range counterpart,
238 seen in Fig. 2(I), but with poorer spatial resolution. Also, the infrared image presented in Fig. 4(I) has a
239 lower spatial resolution and brightness compared to the infrared images reported previously by Kostinskiy
240 et al. (2015 a,b). This is because in the present study images were taken from 2.5 times greater distance,
241 resultant images had 4 times fewer pixels, and frame exposure time was 3-4 times longer (with the same
242 lens). Nevertheless, all the main features of the discharge are visible in infrared image shown in Fig. 4(I).

243 The IR brightness (which represents the energy input to gas) of the channel segments within UPF is similar
244 to that on the channel of upward positive leader, as evidenced by IR brightness profiles shown in Fig. 4(II)
245 for two cross-sections labeled [1] and [2] in Fig. 4(I). The 2D length of the leader channel without taking
246 into account the branching in the IR image from the starting point on the grounded sphere to the most
247 distant point was about 42 ± 1 cm, which, given the 2.4-ms exposure time, is the total leader channel
248 length for this event. It is longer than 29 ± 2 cm in the visible-range image by 10 cm or so.

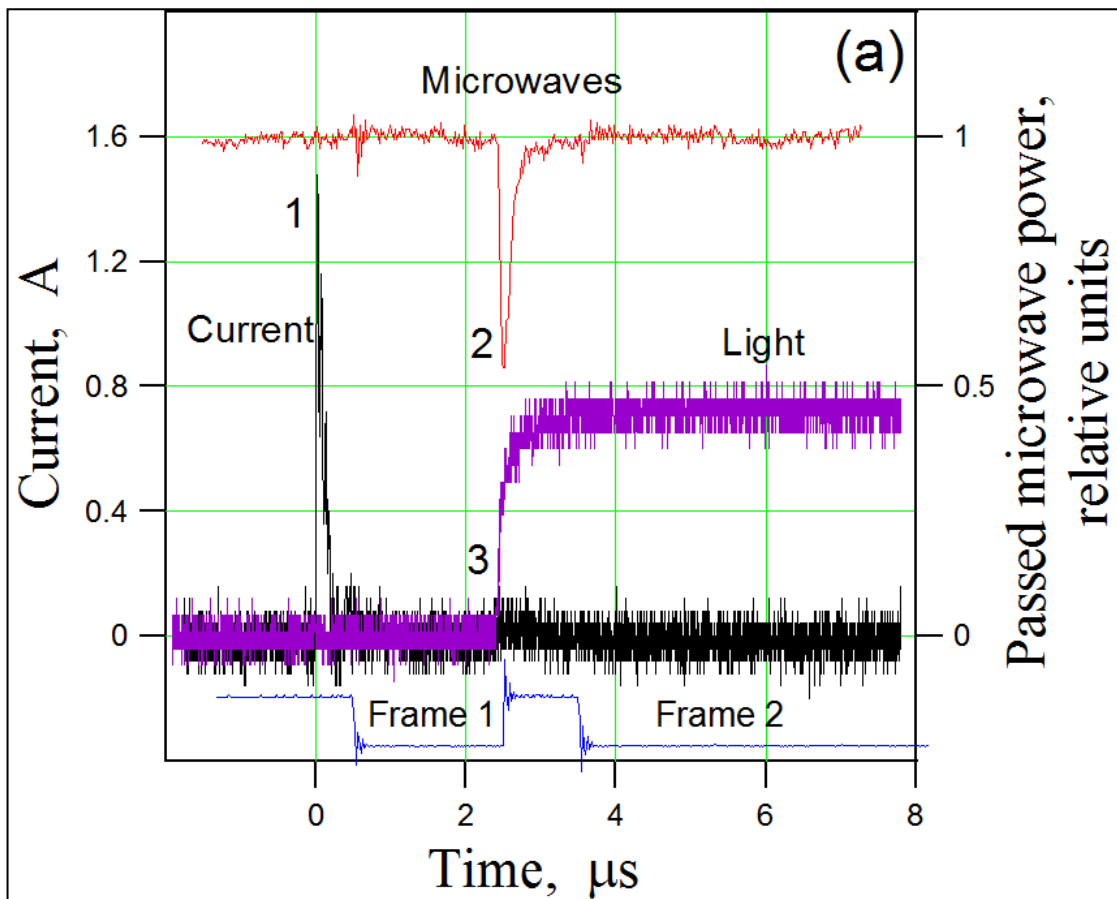
249 We now present an additional event for which the current, light (photomultiplier signal), and microwave
250 absorption were recorded (see Fig. 5a) along with a UPF image (see Fig. 5b). In contrast with the event
251 presented in Figs. 2-4, no leader channel was formed after the initial corona streamer burst. In this case,
252 40 μ s before the initial corona streamer burst and 160 μ s after it, microwave absorption and current
253 measured at the grounded sphere do not indicate any discharge activity. The current signature of the
254 initial corona streamer burst is a single submicrosecond-scale pulse labeled 1 in Fig. 5a. Fig. 5b shows part
255 of the streamer burst (1) that originated on the grounded sphere (2) and propagated to the visible edge
256 of the cloud (3), entered the cloud, and approached almost perpendicularly the region of passage of the
257 microwave beam (5). The streamer heads propagated from the grounded sphere (2) to the microwave
258 beam (5) along an arc distance of about $S_{st} \approx 1.2$ m in about $\tau_{st} \approx 2.4$ μ s (measurement accuracy ± 50 ns). The
259 streamer movement inside the cloud is confirmed by the microwave absorption pulse labeled 2 in Fig. 5a.
260 The microwave absorption pulse duration (FWHM) was slightly longer than in Fig. 3b and was equal to
261 160 ± 20 ns. The absorption pulse peak was very close to the end of exposure of the 4Picos frame shown
262 in Fig. 5b. The average 2D speed of streamers in this case was slightly lower than in Fig. 2 and was equal
263 to $v_{st} \approx S_{st}/\tau_{st} \approx 5 \times 10^5$ m/s. In Fig. 5b, bright channel segments (labeled 4 in Fig. 5b) are seen within the UPF,
264 near the edge of the cloud. The exposure of the first frame of 4Picos (see Fig. 5b) started about 600 ns
265 after the onset of the initial corona streamer burst (see current pulse 1 and the leading edge of the
266 exposure pulse corresponding to Frame 1 in Fig. 5a); that is, the beginning of the streamer burst was not
267 captured by the 4Picos camera. This is why the lower part of the streamer burst (corresponding to the
268 first 600 ns of its development) appears to be missing in Fig. 5b. Note that in Fig. 2(I), the image of
269 streamer burst corresponds to three current pulses labeled 1, 2, and 3 in Fig. 3b.

270 The current pulse 1 (see Fig. 5a) associated with the streamer burst has a peak of about 1.5 A (the rise
271 time of the current pulse is 35 ± 5 ns, the duration of the current pulse at half maximum (FWHM) is $100 \pm$
272 10 ns, and the fall time is 190 ± 10 ns). The total charge of the initial corona streamer burst (estimated by
273 integration of measured current) was about 0.3 μ C, very small compared to the expected cloud charge of
274 about 60 μ C. Relatively hot segments within the UPF in Fig. 5b do not look as bright as those in Fig. 2(I),

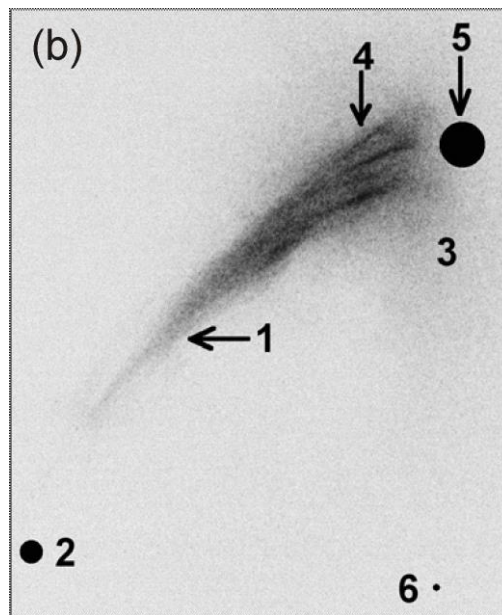


275

276 Figure 4. I (left panel) - One frame of event 2015-12-04_03 obtained with an infrared (FLIR) camera
 277 (wavelength range - 2.5-5.5 μm , image size 320x256 pixels, pixel size 14x15 μm , image depth - 14 bit,
 278 frame exposure - 2.4 ms, lens focal length - 50 mm, f/2). This infrared image was obtained by subtracting
 279 the previous frame from this frame and inverting the differential image; II (right panel) - The IR brightness
 280 profiles for hot channel segments within UPF (shown in blue and labeled [1]) and upward positive leader
 281 channel (shown in red and labeled [2]), with the corresponding cross-sections being shown in I (left panel).
 282 Numbered in I (left panel) are: 3 — negatively charged cloud; 4 — upward positive leader; 5 — streamer
 283 zone of the upward positive leader; 6 — initial corona streamer burst converted to UPF; 7 — hot channel
 284 segments within UPF; 8 — grounded metal sphere (drawn to scale); 9 — center of the grounded plane,
 285 where the nozzle (see Fig. 1) is located; 10 — the region of passage of the microwave beam (drawn to
 286 scale).



287



288

289 Figure 5 (event 14_2015-12-04). (a) Current measured at the grounded sphere (shown in black);
 290 absorption of microwave radiation that passes through the cloud (shown in red and labeled
 291 "Microwaves"); photomultiplier signal (shown in purple and labeled "Light"), and exposure times of 4Picos
 292 Frames 1 and 2 (shown in blue), (b) 4Picos Frame 1 (there is no image in Frame 2). 1 – initial corona
 293 streamer burst converted to UPF; 2 - grounded metal sphere (drawn to scale); 3 - visible boundary of the
 294 cloud of negatively charged water droplets; 4 – hot channel segments within UPF; 5 - the region of passage
 295 of the microwave beam (drawn to scale); 6 - center of the grounded plane, where the nozzle (see Fig. 1)
 296 is located.

297

298 because they were formed at the end of exposure of the 4Picos frame, as evidenced by the
299 photomultiplier and microwave absorption signals, labeled 3 and 2 in Fig. 5a, respectively.

300 **Discussion and Summary**

301 We observed that UPFs, first reported by Kostinskiy et al. (2015a), occurred when the initial (positive)
302 corona streamer burst, initiated from the small grounded sphere, approached and entered the cloud of
303 negatively charged water droplets. In contrast with ordinary streamer formations (e.g., initial corona
304 streamer burst), UPFs contain presumably hot channel segments that are as bright as leader channels in
305 our infrared records and persist for milliseconds (it is in this sense that we refer to them as “hot”; their
306 temperature is actually not known). Importantly, the UPFs occurred prior to the formation (or in the
307 absence) of associated hot leader channel. From this observational fact, we conclude that some kind of
308 streamer-to-leader transition within the initial corona streamer burst is one of the mechanisms behind
309 UPFs. The estimated electric field strength near the cloud boundary was in the range of 500-1000
310 kV/(m·atm). It is presently not clear if the UPFs were caused solely by the enhanced electric field near the
311 charged cloud boundary or other factors also played a role. Within 40 μ s prior to the onset of the initial
312 corona streamer burst, no events that could give rise to UPFs were detected. We infer that the streamer
313 burst entering the cloud experienced some kind of instability (for example, thermal-ionizational instability
314 (Nighan, 1977; Raizer, 1991, pp. 222-226; Bychkov et al., 2007; Zhong et al., 2019; Wolf et al., 2020)) that
315 led to its conversion to UPF.

316 Using current and low-light recordings in conjunction with the microwave sounding of the cloud, we found
317 that hot channel segments within UPFs were formed in very short times of the order of 1 μ s or less. These
318 times are consistent with the characteristic time of development of the streamer-to-leader transition in
319 air at atmospheric pressure (Bazelyan et al., 2007; Popov, 2009). Note also that Suzuki (1971) found, from
320 laboratory experiments with discharges in 1- to 4-cm positive point-to-plane gaps, that thermalization
321 (streamer-to-arc transition) occurred in several hundred nanoseconds, provided that overvoltage
322 exceeded 30%.

323 In this work, we observed hot channel segments embedded in UPFs, which in part were outside the cloud
324 boundary seen with the visible-range camera. It is likely that the space charge is present not only inside,
325 but also outside of the visible cloud, which can explain those observations. It is worth noting that the hot
326 channel segments within UPF always appear in groups, which probably implies that the occurrence of one
327 such segment creates conditions facilitating the occurrence of additional ones.

328 The main findings can be summarized as follows:

- 329 1. Unusual plasma formations (UPFs) can occur inside the initial corona streamer burst, before the
330 development (or in the absence) of hot leader channel.
- 331 2. UPFs contain hot channel segments that are formed, possibly via thermal-ionizational instability, on a
332 time scale of the order of 1 μ s or less.
- 333 3. UPFs tend to occur in the vicinity of cloud boundary, where the electric field is highest, as this boundary
334 is penetrated by the streamer burst.

335 **Acknowledgments**

336 The authors are grateful to the Russian Science Foundation grant No.19-17-00218 for supporting this
337 research and to Ekaterina Svechnikova for help in preparing Figures. The microwave diagnostics work
338 was supported in part by the Russian Science Foundation grant No.19-19-00501.

339 **References**

- 340 Antsupov, K. V., I. P. Vereshchagin, M. A. Koshelev, L. M. Makalsky, and V. S. Syssoev (1991),
341 Discharges from cloud of charged aerosol, in Proc. 7th Int. Symp. on High Voltage Engineering,
342 pp. 15-17, Tech. Univ. of Dresden, Dresden, Germany.
- 343 Bazelyan, E. M. & Raizer, Y. P. (1998). Spark discharge (p. 294). Boca Raton, FL: CRC Press.
- 344 Bazelyan, E.M., Yu.P. Raizer and N.L. Aleksandrov (2007), The effect of reduced air density on
345 streamer-to-leader transition and on properties of long positive leader J. Phys. D: Appl. Phys. 40,
346 4133–4144 doi:10.1088/0022-3727/40/14/007.
- 347 Bogatov, N. A., Kostinskiy, A. Y., Syssoev, V. S., Andreev, M. G., Bulatov, M. U., Sukharevsky, D. I.,
348 Mareev, E.A., & Rakov, V. A. (2020). Experimental investigation of the streamer zone of long-
349 spark positive leader using high-speed photography and microwave probing, J. Geophys. Res.
350 Atmos., 123, e2019JD031826. <https://doi.org/10.1029/2019JD031826>
- 351 Bychkov, V.L., L.P. Grachev, and I.I. Isakov (2007), Thermal Ionization Instability of an Air
352 Discharge Plasma in a Microwave Field, Technical Physics, Vol. 52, No. 3, pp. 289–295.
- 353 Iudin, D.I., V.A. Rakov, A.A. Syssoev, A.A. Bulatov, and M. Hayakawa (2021), From Decimeter-Scale
354 Elevated Ionic Conductivity Regions in the Cloud to Lightning Initiation, Nature Sci. Rep.,
355 doi:10.1038/s41598-021-97321-4 (scheduled for publication at [www.nature.com/articles/s41598-021-](http://www.nature.com/articles/s41598-021-97321-4)
356 [97321-4](http://www.nature.com/articles/s41598-021-97321-4) on Sept. 9, 2021).
- 357 Kossyi I.A., Kostinsky A.Y., Matveev A.A. and Silakov V.P. (1992) Kinetic scheme of the
358 nonequilibrium discharge in nitrogen–oxygen mixtures Plasma Sources Sci. Technol. 1(3) 207.
- 359 Kostinskiy, A.Yu., V. S. Syssoev, N.A. Bogatov, E.A.Mareev, M. G.Andreev, L. M.Makalsky, D. I.
360 Sukharevsky, and V. A. Rakov (2015a), Observation of a new class of electric discharges within
361 artificial clouds of charged water droplets and its implication for lightning initiation within
362 thunderclouds, Geophys. Res. Lett., 42, 8165–8171, doi:10.1002/2015GL065620.
- 363 Kostinskiy, A. Yu., V. S. Syssoev, N. A. Bogatov, E. A. Mareev, M. G. Andreev, L. M. Makalsky, D. I.
364 Sukharevsky, and V. A. Rakov (2015b), Infrared images of bidirectional leaders produced by the
365 cloud of charged water droplets, J. Geophys. Res. Atmos., 120, 10,728–10,735,
366 doi:10.1002/2015JD023827.
- 367 Kostinskiy, A. Yu., Syssoev, V. S., Bogatov, N. A., Mareev, E. A., Andreev, M. G., Bulatov, M. U., et
368 al. (2018). Abrupt elongation (stepping) of negative and positive leaders culminating in an intense
369 corona streamer burst: Observations in long sparks and implications for lightning, J. Geophys.
370 Res. Atmos., 123, doi: 10.1029/2017JD027997.
- 371 Kostinskiy, A. Yu., V. S. Syssoev, N. A. Bogatov, E. A. Mareev, M. G. Andreev, M. U. Bulatov, L. M.
372 Makal'sky, D. I. Sukharevsky, and V. A. Rakov (2016), Observations of the connection of positive
373 and negative leaders in meter-scale electric discharges generated by clouds of negatively charged
374 water droplets, J. Geophys. Res. Atmos., 121, doi:10.1002/2016JD025079.
- 375 Kostinskiy, A. Y., Marshall, T. C., & Stolzenburg, M. (2020), The mechanism of the origin and
376 development of lightning from initiating event to initial breakdown pulses (v.2), J. Geophys. Res.
377 Atmos., 125, e2020JD033191, <https://doi.org/10.1029/2020JD033191>.

- 378 Nighan, W.L. (1977), Causes of thermal instability in externally sustained molecular discharges,
379 Phys. Rev. A, Vol. 15, Number, 1701-1720.
- 380 Popov N.A. (2009), Study of the Formation and Propagation of a Leader Channel in Air, Plasma
381 Physics Reports, Vol. 35, No. 9, pp. 785–793.
- 382 Raizer, Y.P. (1991), Gas Discharge Physics, Springer, Berlin.
- 383 Suzuki, T. Transition from the primary streamer to the arc in positive point-to-plane corona. J.
384 Appl. Phys. 2003, 42, 3766–3777.
- 385 Wolf, A.J., T.W.H. Righart, F.J.J. Peeters, W.A. Bongers, and M.C.M. van de Sanden (2020),
386 Implications of thermo-chemical instability on the contracted modes in CO₂ microwave plasmas,
387 Plasma Sources Sci. Technol. 29, 025005, 11 p.
- 388 Zhong, H., M.N. Shneider, M.S. Mokrov, and Y. Ju (2019), Thermal-chemical instability of weakly
389 ionized plasma in a reactive flow, J. Phys. D: Appl. Phys., 52, 484001, 9 p.